



Universiteit  
Leiden  
The Netherlands

## **MicroRNA-based gene therapy for Huntington's disease : Silencing the villain**

Miniarikova, J.

### **Citation**

Miniarikova, J. (2019, January 24). *MicroRNA-based gene therapy for Huntington's disease : Silencing the villain*. Retrieved from <https://hdl.handle.net/1887/68333>

Version: Not Applicable (or Unknown)

License: [Licence agreement concerning inclusion of doctoral thesis in the Institutional Repository of the University of Leiden](#)

Downloaded from: <https://hdl.handle.net/1887/68333>

**Note:** To cite this publication please use the final published version (if applicable).

Cover Page



Universiteit Leiden



The handle <http://hdl.handle.net/1887/68333> holds various files of this Leiden University dissertation.

**Author:** Miniarikova, J.

**Title:** MicroRNA-based gene therapy for Huntington's disease : Silencing the villain

**Issue Date:** 2019-01-24

4

# **THERAPEUTIC MICRORNAS TARGETING NUCLEAR HUNTINGTIN FOR A DEVELOPMENT OF A PERSONALIZED GENE THERAPY FOR HUNTINGTON'S DISEASE**

**Jana Miniarikova<sup>1,2</sup>, Marina Sogorb-Gonzalez<sup>1,2</sup>, Astrid Vallès<sup>1</sup>, Melvin M. Evers<sup>1</sup>, Harald Petry<sup>1</sup>, Sander J. van Deventer<sup>1,2</sup>, Pavlina Konstantinova<sup>1</sup>**

<sup>1</sup>Department of Research & Development, uniQure, Amsterdam, the Netherlands

<sup>2</sup>Department of Gastroenterology and Hepatology, Leiden University Medical Center,  
Leiden, the Netherlands

## ABSTRACT

Huntington's disease (HD) is a monogenic neurodegenerative disorder caused by an expansion of CAG repeats in the huntingtin (*HTT*) gene, resulting in a formation of a toxic mutant HTT protein. Currently, there is no disease-modifying treatment available. HTT lowering therapies targeting HTT DNA or RNA show a great promise since they offer a reduction of the HD culprit, the mutant HTT protein. One of the most preclinically advanced HTT lowering therapy is a micro (mi)RNA-based gene therapy delivered to target cells by adeno-associated viral (AAV) vectors and resulting in a long-term HTT lowering. The long-perceived theory of miRNA-based lowering occurring predominantly in the cytoplasm is nowadays being questioned, with emerging evidence of miRNAs being active also in the nucleus. A four-nucleotide deletion  $\Delta$ ACTT (rs72239206) in HTT intron 22 is often associated with the mutant HTT in HD patients of A1 haplotype. Here, we investigated the efficacy of therapeutic miRNAs targeting sequences in HTT intron 22 containing  $\Delta$ ACTT to induce nuclear allele-specific mutant HTT lowering. Our results demonstrate a strong mutant HTT protein lowering in HD patient neuronal cultures heterozygous for  $\Delta$ ACTT induced by the miACTT2 construct delivered by an AAV serotype 5 (AAV5) vector. This is a first preclinical evidence suggesting that a therapeutic miRNA can lower the nuclear disease-related transcripts and thereby prevent the translation into the toxic protein. Further experiments are required to confirm a broad applicability. This offers a new perspective on the general application of miRNA-based therapies and their competitiveness with therapies targeting nuclear disease-linked transcripts, such as antisense oligonucleotides.

## INTRODUCTION

Huntington's disease (HD) is a neurodegenerative genetic disorder inherited in an autosomal dominant manner with a prevalence of 1-10 in 100.000 people worldwide.<sup>1</sup> HD pathology results from an expansion of CAG triplet nucleotides in exon 1 of the huntingtin (*HTT*) gene.<sup>2</sup> As a result, mutant HTT protein incorporates an extended polyglutamine (polyQ) chain at the N-terminus. Due to the presence of more than 39 glutamines in the polyQ chain, the mutant HTT misfolds and aggregates, which negatively affects several cellular pathways, causing cellular stress, and ultimately resulting in neuronal cell death over the years.<sup>3,4</sup> Although mutant HTT is expressed throughout the body and peripheral signs of the disease have been also reported, HD is predominantly a disease of the brain, in particular of the striatum and cortex.<sup>5</sup> In most cases, HD manifests in the prime of adulthood with a median survival of 15-18 years after motor symptom onset.<sup>4</sup> The progressive clinical symptoms of HD include motor, cognitive, and psychiatric disturbances.<sup>6</sup> Currently, there is no disease-modifying treatment available.

The gain of toxic function of the mutant HTT protein is widely accepted as a predominant cause of HD pathology.<sup>7</sup> Transgenic HD murine models expressing mutant HTT fragments, causing intracellular formation, develop HD-like neurodegeneration.<sup>8,9</sup> Interference with mutant HTT aggregation results in a suppression of neurodegeneration in HD rodent models.<sup>10-14</sup> Mutant HTT aggregates have been also found *post mortem* in HD human brains.<sup>15,16</sup> HTT lowering therapies that aim to suppress the production of the mutant HTT protein represent the main therapeutic approach towards HD.<sup>17</sup> Many studies in small and large animals have tested the efficacy of (mutant) HTT lowering technologies based on antisense oligonucleotides or RNA interference (RNAi).<sup>Reviewed in 18-20</sup> In contrast to antisense oligonucleotides that demonstrated short-term (in months) HTT lowering, RNAi molecules delivered by viral vectors offer an advantage of a continuous long-term (in years) HTT lowering.<sup>17</sup> One of the most advanced RNAi approaches applies intra-striatal delivery of adeno-associated viruses (AAVs) to express therapeutic micro (mi)RNA precursors.<sup>11</sup> These precursors are processed by the cellular RNAi machinery, generating a mature therapeutic that binds to HTT transcripts and suppresses HTT translation.<sup>21</sup> The safety and efficacy of various therapeutic miRNAs have been preclinically evaluated in rodent and large HD animal models and currently they are approaching clinical testing.<sup>11,13,22-25</sup>

The traditional concept of cellular miRNAs being active mainly in the cytoplasm has been challenged in recent years as systematic profiling analyses performed on RNA isolated from the nuclear and cytoplasmic fractions demonstrated that a majority of cellular miRNAs are present in the nucleus.<sup>26-29</sup> Moreover, the cardinal proteins enabling RNAi in the cytoplasm such as AGO2, Dicer1, TRBP2 and GW182 have been recently also found in the nucleus.<sup>30</sup> AGO2 catalytic activity is preserved in nuclear extracts, indicating the possible functionality of AGO2-bound miRNAs in the nucleus. This provides opportunities to design therapeutic miRNAs targeting nuclear disease-related transcripts.

As HD is a rare disease with a dominant inheritance, the homozygous HD mutation carriers are only occasional and most HD patients express the wild-type and mutant HTT.<sup>31</sup> Dozens of heterozygous single-nucleotide polymorphisms (SNPs) have been identified that are *in cis* with the HD mutation and largely annotate HD haplotypes.<sup>32</sup> These heterozygous SNPs allow for a design of miRNAs to induce the allele-specific lowering. Unfortunately, allele-specific lowering has limitations because 1) the treatment needs to be personalized and therefore, currently, it would be available only for specific subgroups of HD patients, and 2) the allele-selectivity-to-efficacy ratio does not outweigh the efficacy level induced by the non-selective approach, which is the deciding factor for the efficacy of current gene therapy approaches. Recently, a deletion of four nucleotides  $\Delta$ ACTT (rs72239206) in HTT intron 22 has been identified in the most frequent heterozygous HD haplotype A1 in Canadian Caucasian population.<sup>32</sup>  $\Delta$ ACTT is located in the intronic region, which suggests that most of the  $\Delta$ ACTT-containing transcripts are located in the nucleus, before the splicing occurs. Hence, the  $\Delta$ ACTT deletion offers the opportunity to simultaneously evaluate the allele-specific and nuclear HTT lowering.

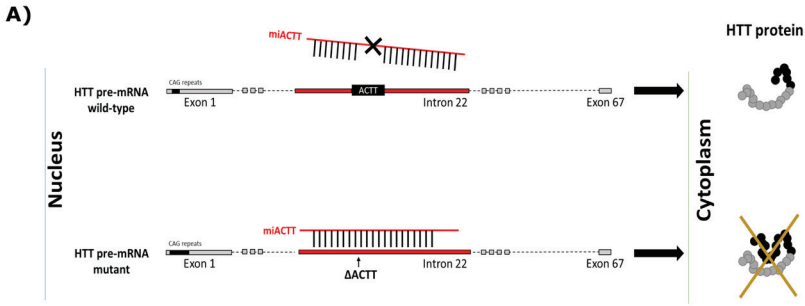
The aim of this study was to demonstrate the efficacy of therapeutic miRNAs to lower the nuclear mutant HTT transcripts. We designed therapeutic miRNAs (referred as miACTTs) to target mutant HTT sequences located in HTT intron 22 encompassing  $\Delta$ ACTT. We hypothesized that targeting  $\Delta$ ACTT will offer a greater mutant selectivity compared to the standard SNP-based approaches, which strongly depends on the number of nucleotides not matching to the wild-type HTT sequences. We designed two artificial miRNAs (miACTTs) embedded in five different endogenous pre-miRNA precursors, and their allele-selectivity was first addressed using luciferase reporter constructs. The HTT lowering activity of several miACTTs was evaluated in both nucleus and cytoplasm and we analyzed the processing of mature miACTT, allowing a selection of a candidate that was devoid of passenger strand activity. The efficacy and allele-selectivity of the most efficient miACTT2 candidate embedded in the hsa-miR-451 precursor delivered by an AAV5 vector was evaluated in induced pluripotent stem cells (iPSC)-derived HD neuronal cultures heterozygous for  $\Delta$ ACTT.

## RESULTS

### **Therapeutic miRNAs show strong allele-selective lowering of luciferase reporters heterozygous for $\Delta$ ACTT (rs72239206).**

To design therapeutic miRNAs that effectively and selectively target  $\Delta$ ACTT (rs72239206) in HTT intron 22, we analyzed a sequence composition in the HTT gene region surrounding  $\Delta$ ACTT (**Figure 1a**). We searched for enriched AT motifs to identify the beginning of the 5' end of the guide strand while keeping  $\Delta$ ACTT binding either at the 3' end or in the center of the pre-miRNA. Enriched AT motifs at the beginning of a guide strand have been shown to reduce the production of the passenger strand during the pre-miRNA processing and reducing the odds of passenger strand-related unwanted off-target interactions.<sup>11,20</sup> Moreover, 3' end or central positions of the target nucleotides during the target miRNA-mRNA binding have been shown to improve the allele-selectivity of the artificial miRNAs by reducing thermodynamic stability between the miRNA and mismatch mRNAs.<sup>11</sup> We identified two regions that contain five nucleotide-long AT motifs with the  $\Delta$ ACTT binding starting at position 19 and 9 from the 5' end of the guide strand, named miACTT1 and miACTT2. We placed miACTT1 and miACTT2 guide strands in five scaffolds that we have previously evaluated with an artificial miRNA targeting HTT exon 1: hsa-miR-101, hsa-miR-122, hsa-miR-135, hsa-miR-155, and hsa-miR-451.<sup>11</sup> The passenger strands were corrected to maintain the original miRNA scaffolding. The resultant constructs are named miACTT1-101, miACTT1-122, miACTT1-135, miACTT1-155, miACTT2-101, miACTT2-122, miACTT2-135, miACTT2-155, and miACTT2-451 (**Figure 1b**). To address the efficacy of the miACTT constructs, we generated a renilla luciferase reporter expressing a luciferase gene fused with HTT intron 22 containing  $\Delta$ ACTT and the splicing sites, named Luc- $\Delta$ ACTT (**Figure 1c**). To address the allele-selectivity of miACTTs, we generated a second renilla luciferase reporter containing HTT intron 22, named Luc-ACTT. All miACTT constructs perfectly match to Luc- $\Delta$ ACTT and have a four-nucleotide mismatch with Luc-ACTT.

To evaluate the efficacy and allele-selectivity of the miACTT constructs, we co-transfected them with Luc-ACTT and Luc- $\Delta$ ACTT reporters in HEK293T cells and quantified the luciferase activity. We observed 60-90% lowering of Luc- $\Delta$ ACTT reporter activity as compared to 20-40% lowering of the Luc-ACTT activity by all miACTT constructs, demonstrating strong allele-selectivity (**Figure 1d**). Overall, miACTT1 constructs showed slightly stronger allele-selectivity compared to miACTT2 constructs, confirming that the 3' end terminal binding interaction between the miRNA and target mRNA is more potent to discriminate a four-nucleotide mismatch.



**B)**

**miACTT1-101**

```

u   cu agc   acacguuuuucuguuaa   c   gucu a
gcc   acacguuuuucuguuaa   aacu   u
cgg   uugcauuuuagcauuu   ugg   aaauc
a   uaggc   -   -   -   -   -   -
    
```

**miACTT1-122**

```

c   -   uu   u   ugucu
cuuagcag   agcugu   uaacaga   aaucguguca   ugucu   a
ggaucguc   ucgaa   auugucu   uauugcacagu   uauca
c   a   cc   c   -   -   -   -
    
```

**miACTT1-135**

```

----- ca   -   uaa   -   -   cu
cucu   gcuguggcc   uuuuaacaga   uacgugucac   uug   g
ggga   ugacauc   gaaaaauugucu   augcacagug   aac   u
ccucgagcg   g   uci   -   ca   cc
    
```

**miACTT1-155**

```

c   a   c   u   -   c
cuguuuuaacagaua   ua   gugucacu   uug   c
gacaaaauugucuau   au   cacagugg   aac   u
c   -   -   -   -   uc   c
    
```

**miACTT2-101**

```

u   cuggc   uuuguuugugacacguau   c   gucu a
gcc   uuuguuugugacacguau   uacu   u
cgg   aaacaaacacugugcaua   augg   u
a   uaggc   -   -   -   -   -   -
    
```

**miACTT2-122**

```

c   aa   c   ugucu
cuuagcag   agcugu   uacgugu   acaaacaaaa   a
ggaucguc   ucgaa   augcaca   uguuuuuuuuu   a
c   a   cc   c   -   -   -   -   uauca
    
```

**miACTT2-135**

```

----- ca   -   cac   -   -   cu
cucu   gcuguggcc   uaaucgugu   aaacaaaaau   uug   g
ggga   ugacauc   gaaauugcaca   uuuguuuuuu   aac   u
ccucgagcg   g   cci   -   ca   cc
    
```

**miACTT2-155**

```

c   c   a   a   u   -   c
cuguuuuaacgugu   acaa   caaaaauu   uug   c
gacuuuugcaca   uguu   guuuuuag   aac   u
c   -   -   -   -   uc   c
    
```

**miACTT2-451**

```

c   a   gu   a   a
uuggg   auggcaag   aaucgugucacaaaa   a
gacc   uaucguuc   uauugcacaguguuuuu   a
a   a   ac   a
    
```

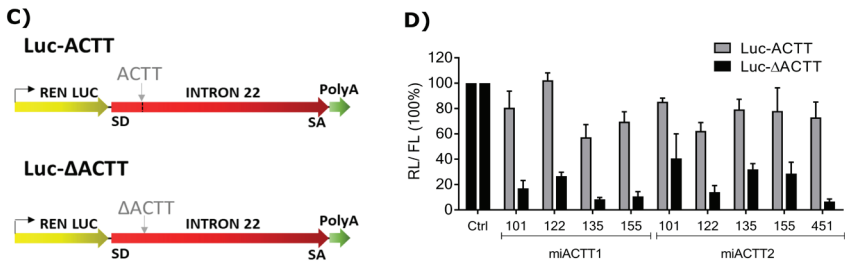


**Figure 1. miACTT1 and miACTT2 precursors induce strong allele-selective lowering of luciferase reporters carrying HTT intron 22 with  $\Delta$ ACTT.** (A) Proposed mechanism of action for miACTT1 and miACTT2 guide sequences targeting HTT intron 22 containing  $\Delta$ ACTT. miACTTs bind to HTT intron 22 with  $\Delta$ ACTT based on miRNA-mRNA complementarity in the nucleus. It results in an overall reduction of the mutant HTT protein in the cytoplasm. (B) The schematic of miACTT1 and miACTT2 guide sequences embedded in five human pre-miRNA scaffolds, named miACTT1-101, miACTT1-122, miACTT1-135, miACTT1-155, miACTT2-101, miACTT2-122, miACTT2-135, miACTT2-155, and miACTT2-451. Based on miRBase database ([www.mirbase.org](http://www.mirbase.org)), the guide and passenger strands are represented in red and blue, respectively. (C) Schematic of luciferase reporters containing renilla luciferase gene (REN LUC) fused to HTT intron 22 with ACTT, named Luc-ACTT, and with the ACTT deletion, named Luc- $\Delta$ ACTT. (D) Luc-ACTT and Luc- $\Delta$ ACTT luciferase knock-down by miACTT1 and miACTT2 scaffolds in HEK293T cells.

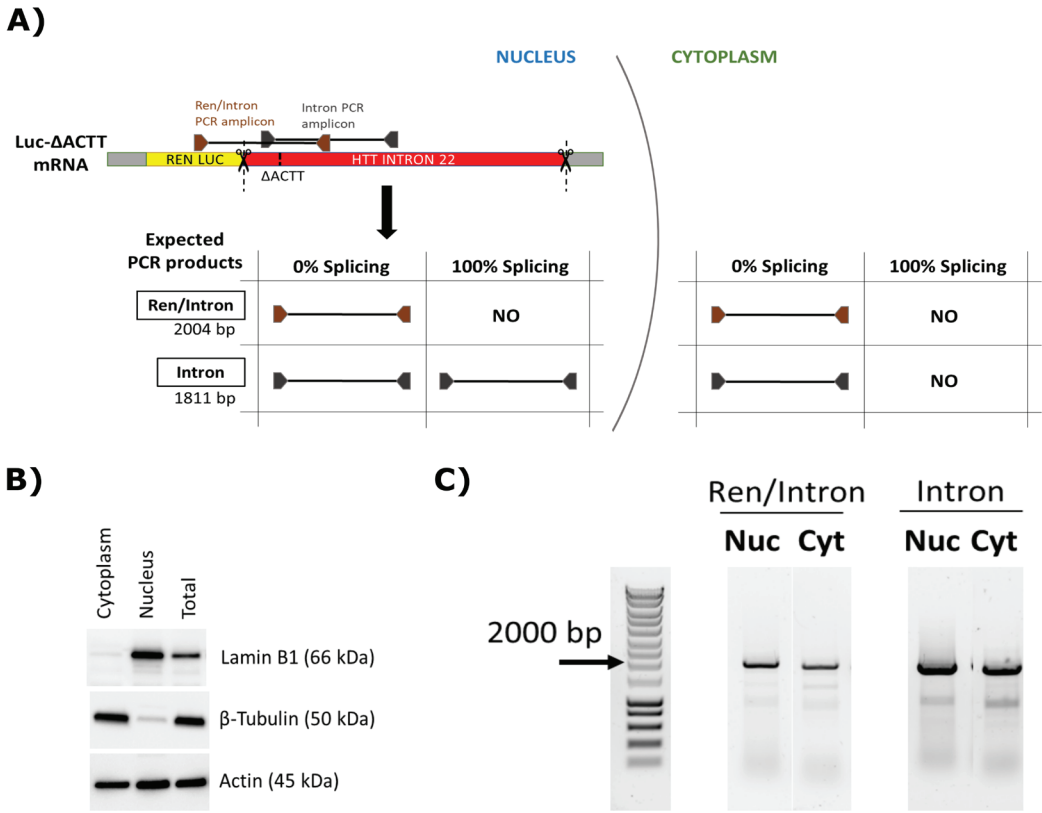
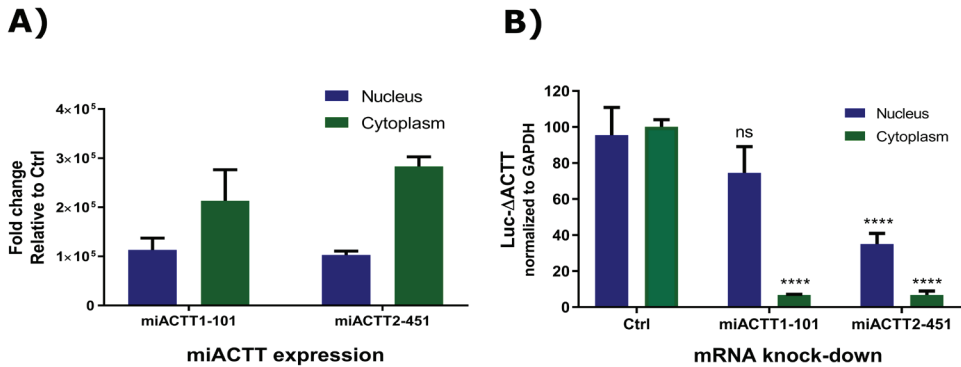


**Figure 2. The Luc- $\Delta$ ACTT reporter expresses renilla transcripts fused with HTT intron 22 in the cytoplasm.** (A) The overview of expected PCR products in case 0% or 100% splicing of HTT intron 22 from the luciferase reporters occurs. Two PCR primer pairs were designed to amplify a fragment encompassing a portion of luciferase gene and HTT intron 22, named Ren/Intron, or a fragment within HTT intron 22, named Intron. (B) Western blotting showing a separation of the nuclear and cytoplasmic fraction. Lamin B1 is an exclusive nuclear protein,  $\beta$ -tubulin is an exclusive cytoplasmic protein, and Actin can be found in all fractions. (C) PCR products using Ren/Intron and Intron primers separated on an agarose gel.

The HTT intron 22 containing the splicing sites is located in the 3'UTR of the luciferase gene and this may interfere with effective splicing. Therefore, we analyzed the splicing efficacy of HTT intron 22 from the Luc- $\Delta$ ACTT reporter by RT-PCR of the nuclear and cytoplasmic RNA fractions isolated from HEK293T cells (Figure 2). We used custom primers that generate an amplicon within the intron 22, named Intron, or an amplicon encompassing a part of the luciferase gene and intron 22, named Ren/Intron (Figure 2a). A separation of the nucleus and cytoplasm was evaluated by western blotting using nuclear marker Lamin B1 and cytoplasmic marker  $\beta$ -Tubulin (Figure 2b). RT-PCR products were separated by electrophoresis on agarose gels (Figure 2c). We detected equal bands of unspliced variants in both cytoplasm and nucleus using both primer sets, suggesting that splicing does not occur or, at such a low rate, that it cannot be visualized on a gel. The inability of HTT intron

22 to be effectively spliced from the luciferase reporter can reflect its placement in the 3'UTR of the luciferase gene. This result indicates that the miACTTs evaluated in this system have the potential to target HTT mRNA in the nucleus and in the cytoplasm. Furthermore, this is also indicative that lowered mRNA in the cytoplasm can be the result of both nuclear and cytoplasmic lowering. To further establish whether the lowering efficacy of luciferase expression is a result of mRNA lowering in the nucleus, we conducted further experiments described below.



Mean CT values

	Nucleus			Cytoplasm		
	GAPDH	Ren/Intron*	Intron*	GAPDH	Ren/Intron*	Intron*
Ctrl	22.1	19.6	20.1	20.3	19.9	20.2
miACTT1-101	22.2	20.1	20.6	20.5	23.4	24
miACTT2-451	21.9	20.7	21.2	20.9	23.8	24.5
NTC	40	29.1	32	40	35.7	33.3

**Figure 3. Luc-ΔACTT mRNA knock-down induced by the miACTT1-101 and miACTT2-451 construct in the nucleus and cytoplasm of HEK293T cells. (A)** Differential expression of mature miACTT1 and miACTT2 molecules measured by RT-qPCR in the nuclear and cytoplasmic fraction using custom TaqMan small RNA probes. **(B)** TaqMan RT-qPCR analysis to evaluate the Luc-ΔACTT knock-down by miACTT1-101 and miACTT2-451 in the nucleus and cytoplasm of HEK293T cells. Mean CT values of Luc-ΔACTT mRNA measured by qPCR in the nuclear and cytoplasmic fractions using Ren/Intron\* and Intron\* TaqMan probes. GAPDH was used as an internal control. Ctrl represents a PBS group and NTC describes a non-template control. All data were analyzed using one-way ANOVA. Data are represented as the mean ± s.d. (error bars) \*\*\*,  $p \leq 0.001$ ; \*\*\*\*,  $p \leq 0.0001$ ; ns= non-significant.

### miACTT1-101 and miACTT2-451 constructs induce mRNA lowering of luciferase reporters in the nucleus and cytoplasm.

We have previously shown that the miR-451 scaffold does not produce any passenger strand *in vitro* and *in vivo*. It limits the chance for off-target activity thereby providing better safety profiles.<sup>10,11</sup> Therefore, the miACTT2-451 construct was investigated in more detail, along with the miACTT1-101 construct that showed the strongest selective efficacy *in*

*vitro*. To further quantify the miACTT expression, HTT intron 22 splicing from the luciferase reporters, and lowering of luciferase reporters within different cellular compartments, we co-transfected miACTT1-101 and miACTT2-451 with the Luc- $\Delta$ ACTT reporter in HEK293T cells and analyzed the expression of their transcripts. Both scaffolds induced  $\sim 1 \times 10^5$  levels of mature miACTT1-101 molecules in the nucleus when normalized to the scrambled negative control (**Figure 3a**). In the cytoplasm, the miACTT2-451 was slightly more abundant ( $\sim 2.8 \times 10^5$ ) compared with miACTT1-101 ( $\sim 2.1 \times 10^5$ ), when normalized to the negative scrambled control. To address the splicing and knock-down efficacy of the Luc- $\Delta$ ACTT reporter, we performed RT-qPCR with TaqMan primers, named Intron\* and Ren/Intron\* (**Figure 3b**). We measured equal values of Luc- $\Delta$ ACTT transcripts with both probes (data shown for Intron\*), suggesting that the splicing of intron 22 from the luciferase reporter indeed does not occur or it is not detectable by RT-qPCR, and the knock-down efficacy should be evaluated separately in the nucleus and cytoplasm. Both miACTT1-101 and miACTT2-451 constructs induced a strong  $\sim 90\%$  knock-down of Luc- $\Delta$ ACTT transcripts in the cytoplasm. However, at an equal expression level within the nucleus, miACTT2-451 construct showed stronger  $\sim 65\%$  silencing of the nuclear Luc- $\Delta$ ACTT as compared to only  $\sim 25\%$  silencing induced by the miACTT1-101 construct, suggesting that the silencing activity of the miACTT constructs in the nucleus is scaffold-dependent.

### **The miACTT2-451 construct does not generate a passenger strand *in vitro*.**

The miACTT1-101 and miACTT2-451 constructs are embedded in different scaffolds and hence they generate different amounts of the guide and passenger strands. To address the processing patterns of these constructs, we performed small RNA next generation sequencing. The overview of the read alignments for the pre-miACTT1-101 and pre-miACTT2-451 constructs are presented in (**Figure 4a**). The analysis of the sequence length and composition revealed that the guide strands from both constructs were cleaved precisely at the predicted Drosha sites, whereas the further downstream Dicer cleavage generated all the variability in the sequence length (**Figure 4b**). This processing pattern is consistent with our previously published studies using different therapeutic miRNAs.<sup>10,11</sup> 47% reads processed from the miACTT1-101 scaffold were 22 nucleotides long. The miACTT2-451 processing generated variable lengths of the reads with 39% reads of 25 nucleotides in length. In case of the pri-miR-451 scaffold, the heterogenous 3' arm is a result of a cleavage by Argonaute 2 (AGO2) and further trimming by PARN.<sup>33,34</sup> With the regard to the miRNA activity, the crucial "seed" region recognizing the mRNA target is positioned in the 5' arm and therefore, the activity is preserved. We confirmed the absence passenger strands generated from the miACTT2-451 constructs, whereas we detected 8% of the passenger strand originating from the miACTT1-101 constructs. Based on the results above, we selected miACTT2-451 scaffold for further testing.

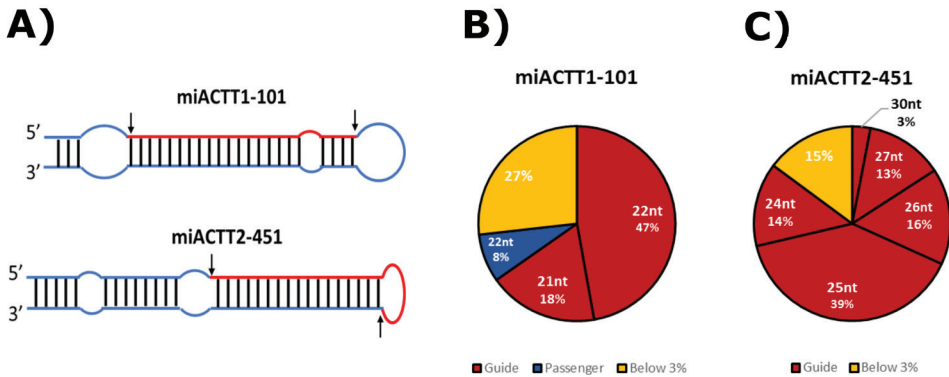


**Figure 4. Next generation sequencing analysis of miACTT1-101 and miACTT2-451 processing in HEK293T cells. (A)** Schematic representation of pre-miACTT1-101 and pre-miACTT2-451 scaffolds. Based on miRBase database ([www.mirbase.org](http://www.mirbase.org)), the guide and passenger strands are represented in red and blue, respectively. Expected Drosha and Dicer guide cleavage sites are represented by arrows. **(B)** The length distribution of reads mapping to pre-miACTT1-101. For the read alignments, up to three mismatches with the references sequence were allowed. Reads represented with less than 3% were excluded from the figure. **(C)** The length distribution of reads mapping to pre-miACTT2-451. For the read alignments, up to three mismatches with the references sequence were allowed. Reads represented with less than 3% were excluded from the figure.

### Genotyping and generation of HD patient-derived neuronal cultures heterozygous for $\Delta$ ACTT

To gain more insights into the efficacy and allele-selectivity of lowering endogenous mutant HTT by the miACTT2-451 construct, we took advantage of recent protocols that enable generation of HD neuronal cultures from HD-derived iPSCs (**Figure 5a**). These iPSCs are reprogrammed from fibroblasts isolated from HD patients and can be differentiated into several neuronal lineages. To date, no HD-derived iPSCs have been reported to be heterozygous for  $\Delta$ ACTT. To identify candidate iPSCs for generation of HD neuronal cultures heterozygous for  $\Delta$ ACTT, seven different HD fibroblast cell lines were tested for  $\Delta$ ACTT heterozygosity: GM02147, GM02155, GM04022, GM04281, GM04717, GM09197, GM21756 (Coriell biorepository) (**Figure 5b**). We identified GM09197 with 180 CAG repeats as the only cell line heterozygous for  $\Delta$ ACTT and obtained iPSCs derived from these cells. As a negative control, not heterozygous for  $\Delta$ ACTT, we selected commonly used iPSCs originating from GM04281 fibroblasts containing 71 CAG repeats. HD neuronal cultures were induced and differentiated from iPSCs that were derived from GM09197 and GM04281 fibroblasts and confirmed differentiation into matured neuronal cultures using the MAP2 marker (**Figure 5c**). The heterozygosity for  $\Delta$ ACTT in HD neuronal cultures was confirmed by performing RT-qPCRs with custom primers detecting  $\Delta$ ACTT or ACTT polymorphism (**Figure 5d**). We also analyzed the matured neuronal cultures for an additional heterozygous (C/T) SNP rs362307 that is also associated with the A1 haplotype and is localized in the 3'UTR of HTT mRNA. In contrast to the  $\Delta$ ACTT polymorphism, SNP rs362307 is localized in the region that is not spliced and thus, this SNP enabled us to test the allele-specific mutant HTT mRNA knock-

down in both the nucleus and cytoplasm. As expected, we detected the presence of both ACTT/ $\Delta$ ACTT and (C/T) rs362307 polymorphisms in neuronal cultures containing 180 CAGs (CAG180), but not in the neuronal cultures with 71 CAGs (CAG71).

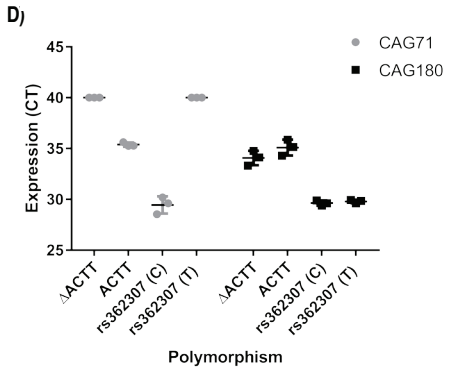
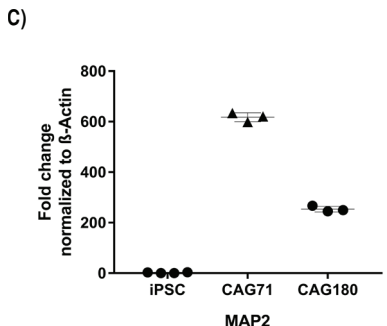
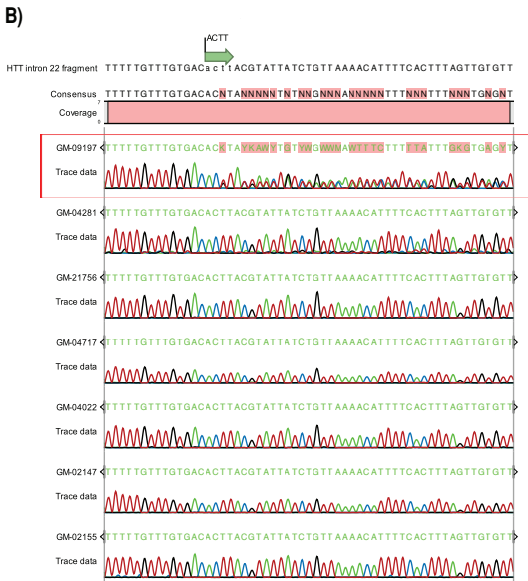
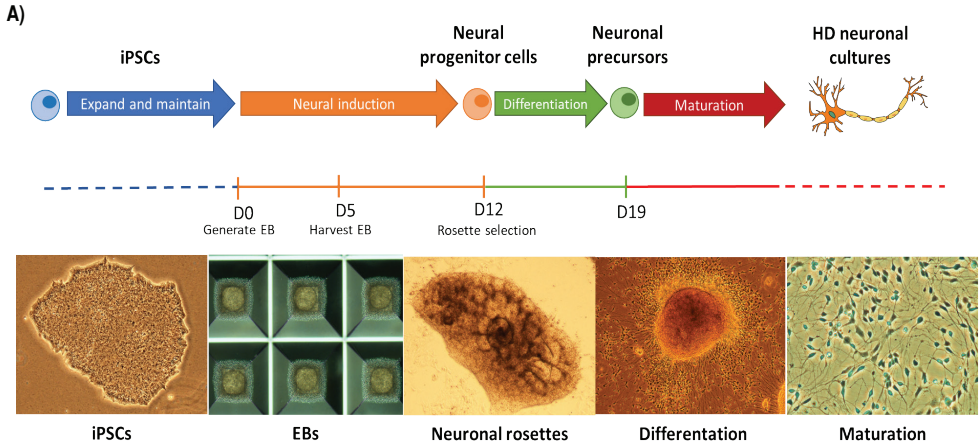


**Figure 5. GM09197 fibroblasts are heterozygous for  $\Delta$ ACTT and identify a source of iPSCs to generate HD neuronal cultures heterozygous for  $\Delta$ ACTT.** (A) An outline of a generation of matured HD-derived neuronal cultures from iPSCs. (B) Sanger sequencing of DNA isolated from seven HD fibroblast cell lines: GM02147, GM02155, GM04022, GM04281, GM04717, GM09197, GM21756. The region of interest is the sequence in HTT intron 22 containing ACTT/ $\Delta$ ACTT polymorphism. GM09197 positive for  $\Delta$ ACTT is highlighted in red. (C) MAP2 immunostainings of two-week matured CAG71 and CAG180 neuronal cultures. (D) RT-qPCR using custom TaqMan probes to evaluate ACTT/ $\Delta$ ACTT or (C/T) rs362307 heterozygosity in matured CAG71 and CAG180 neuronal cultures.

### **AAV5-miACTT2-451 construct induced nuclear HTT lowering in HD neuronal cultures.**

To evaluate the efficacy of endogenous mutant HTT lowering in HD neuronal cultures by the miACTT2-451, we generated an AAV5 virus to deliver the miACTT2-451 expression cassette, named AAV5-miACTT2-451. Three different doses of AAV5-miACTT2-451 ( $1e10$ ,  $1e11$ , and  $1e12$  total genomic copies (gc)) were used to transduce two-week matured CAG71 and CAG180 neuronal cultures (**Figure 6a**). Ten days post-transduction, we analyzed the transduction efficacy by measuring mature miACTT2 expression in the total cell lysates and separately in the cytoplasm and nucleus of CAG180 cells. We detected a dose-dependent increase of mature miACTT2-451 levels in the total cell lysates isolated from CAG71 and CAG180 cells (**Figure 6b**). We observed higher transduction efficacy of CAG71 cells compared with CAG180 cells. Mature miACTT2-451 molecules were  $\sim 3$  times more abundant (fold change  $\sim 670$ ) in the cytoplasm of CAG180 cells compared with the nuclear fraction (fold change  $\sim 200$ ), when normalized to the negative saline control (**Figure 6c**). To address the allele-selective mRNA knock-down by AAV5-miACTT2-451 constructs, we performed TaqMan mRNA assays (**Figure 6d**). We observed  $\sim 40\%$  selective mutant HTT mRNA knock-down at the highest dose of  $1e12$  gc AAV5-miACTT2-451. Ultimately, we addressed the mutant HTT protein knock-down in both CAG71 and CAG180 cells by Singulex assay (**Figure 6e**). All doses induced strong 50-60% mutant HTT knock-down in CAG180 cells and 5-10% knock-down in CAG71 cells. Hence, this is a first report suggesting that artificial miRNAs can be active in the nucleus and can lower the expression of a disease gene in human HD neuronal cultures.

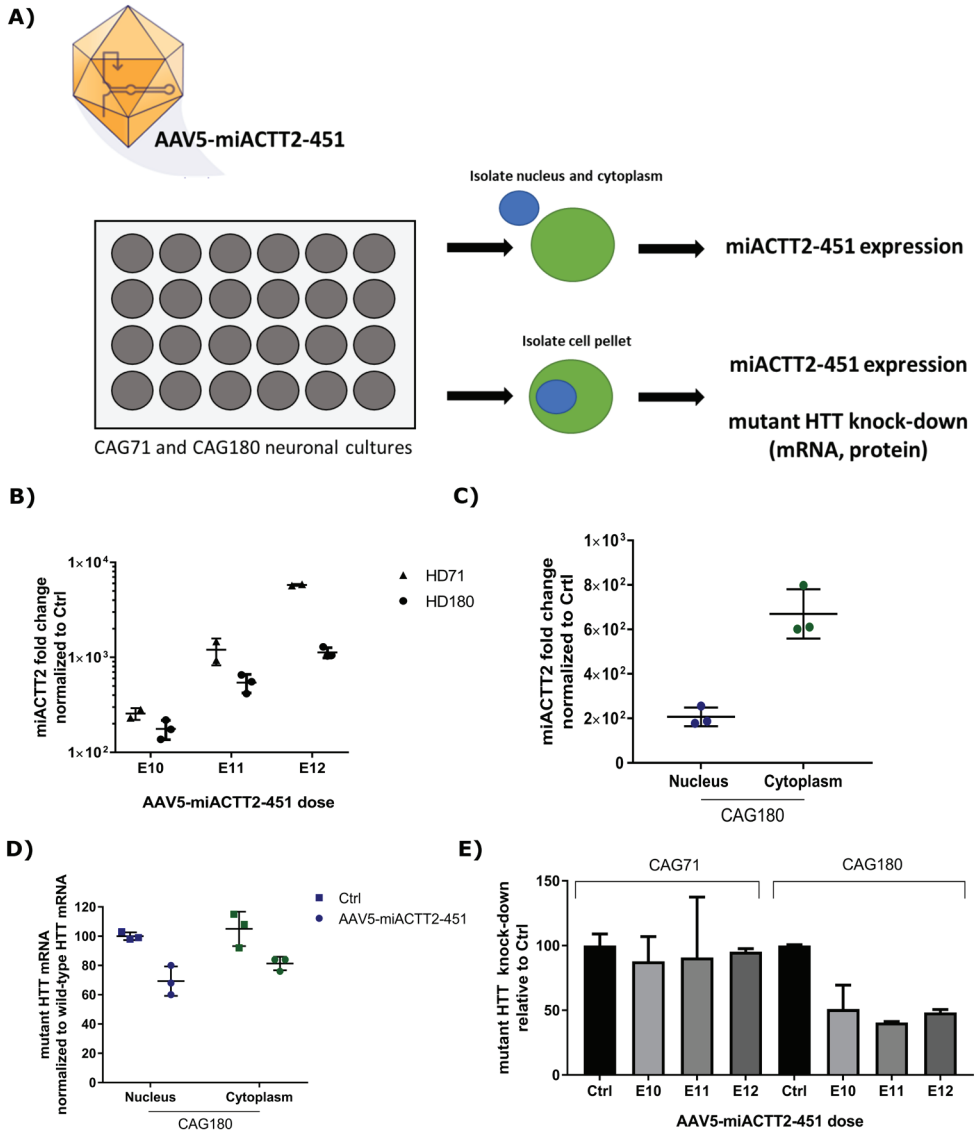


**Figure 6. The mutant HTT lowering induced by the AAV5-miACTT2-451 construct in CAG180 neuronal cultures.** (A) The experimental outline of AAV5 transductions and downstream analysis. (B) The miACTT2 expression in CAG71 and CAG180 cells transduced with E10, E11, and E12 genomic copies of AAV5-miACTT2-451 measured by small RNA TaqMan RT-qPCR. miACTT2 values are presented as a distribution plot with the mean of the values following normalization to U6 levels. (C) The miACTT2 expression in nucleus and cytoplasm of CAG180 cells transduced with E12 genomic copies of AAV5-miACTT2-451 measured by small RNA TaqMan RT-qPCR. The miACTT2 values are presented as a distribution plot with the mean of the values following normalization to U6 levels. (D) The mutant HTT mRNA knock-down in CAG180 cells measured by RT-qPCR using primers detecting (C/T) rs362307 heterozygosity. (E) Mutant HTT protein knock-down in CAG71 and CAG180 cells measured by Singulex SMC Immunoassay.

## DISCUSSION

We here report an evidence of the allele-specific nuclear mutant HTT lowering by artificial miACTT1 and miACTT2 constructs, processed from the pre-miR-101 and pre-miR-451 precursors respectively, and targeting sequences in HTT intron 22 with  $\Delta$ ACTT (rs72239206) polymorphism. We detected mature miACTT1 and miACTT2 sequences in the nucleus and cytoplasm of HEK293T cells. In HD neuronal cultures heterozygous for  $\Delta$ ACTT, the miACTT2-451 construct delivered by the AAV5 vectors resulted in the selective lowering of mutant HTT mRNA and protein. This is a first evidence suggesting that artificial miRNAs can be designed to lower disease-related transcripts in the nucleus and supports further investigations.

There is accumulating evidence that cellular miRNAs and RISC proteins are present and active in the nucleus in many cells types.<sup>35</sup> Several profiling studies have shown that hundreds of miRNAs are present in the nucleus of human neural stem cells, rat neurons, and cancerous cell lines such as HeLa.<sup>29,36,37</sup> In general, nuclear miRNAs have been found two- or four-fold less abundant in the nucleus when compared with the cytoplasm.<sup>28</sup> This is consistent with our current results from HD neuronal cultures, where we found approximately three-fold lower miACTT2 concentrations when compared with the cytoplasm. However, the nuclear concentration of miACTT2 was sufficient to induce 50-60% lowering of mutant HTT protein. Noteworthy, we did not detect a strong HTT mRNA knock-down, which might be reflected by the experimental errata and further experiments are required to address levels of HTT mRNA knock-down in this setting.

miRNAs are a class of small RNAs known to regulate gene expression primarily in the cytoplasm by binding to transcripts and inducing either their degradation or translational repression.<sup>38,39</sup> In the canonical pathway, miRNA processing is initiated in the nucleus where the long pri-miRNA precursor is expressed and processed by Drosha to generate a shorter stem-loop pre-miRNA precursor.<sup>40</sup> The pre-miRNA is subsequently exported out of the nucleus by Exportin 5.<sup>41</sup> In the cytoplasm, a majority of pre-miRNA loops are cleaved by Dicer to generate a double-stranded mature miRNA that is analogous to an siRNA.<sup>42,43</sup> Based on the thermodynamic properties of the 5'ends of the double-stranded miRNA molecules, the passenger strand is selected and degraded by AGO2, enabling the guide strand to be functionally active.<sup>44</sup> In the noncanonical pathway, that has been so far reported for the pre-miR-451 scaffold, the pre-miR-451 stem loop is recognized directly by AGO2, cleaved precisely to generate a thirty-nucleotide long guide molecule and trimmed by PARN to further render a mature miR-451 guide strand.<sup>33,34,45</sup> The non-canonical pathway does not generate a passenger strand and thus, the pre-miR-451 scaffold has been recently proposed by several groups, including ours, for the miRNA and shRNA design since it limits the off-target effects by the passenger strand.<sup>11,46,47</sup> The target recognition and lowering efficacy between miRNA and target mRNA is based on the sequence and level of base-pair

complementarity.<sup>48</sup> In this study, we designed miACTT1 and miACTT2 constructs that have a perfect complementarity with HTT intron 22 carrying  $\Delta$ ACTT and a four-nucleotide mismatch when binding to HTT intron 22 carrying ACTT. Both miACTT constructs showed strong allele selectivity with miACTT1 constructs being slightly more efficient. This can reflect 3' end position of the miACTT1 binding to  $\Delta$ ACTT, which is consistent with our previous studies showing that the terminal binding to the polymorphism can enhance the allele-selectivity.<sup>11</sup> The miACTT2 construct processed from the pre-miR-451 scaffold showed stronger allele-selectivity of luciferase reporter mRNA in the nucleus, when compared to pre-miR-101 scaffold, and no passenger strand, which strongly supports the use of miR-451 scaffold for the therapeutic purposes.

Currently, the most advanced approaches of HTT lowering, including the first clinical trial initiated in 2015 (NCT02519036), target both HTT alleles and thus, provide a potential therapy for all HD patients. Lowering of both HTT alleles by antisense oligonucleotides or RNAi molecules has been shown so far to be an effective HTT-lowering approach and no adverse effects have been observed in HD rodent or large animal models.<sup>17,24,49,50</sup> The ultimate goal of a personalized gene therapy by the selected miACTT2-451 construct is to exclusively lower the expression of the mutant HTT in HD patients and thus, to limit the potential safety concerns of non-selective HTT lowering. The preclinical development of a personalized gene therapy for HD requires to address the efficacy and safety of a therapeutic product in animals before entering the clinic. Although HD animal models are plentiful and commonly used for preclinical testing, the intronic  $\Delta$ ACTT mutation has been only recently discovered and no heterozygous animal model is available. HD patient-derived induced pluripotent stem cells (iPSCs) have emerged as a new disease model which more closely represent the disease genetic background as compared to HD rodents and large animals.<sup>51</sup> In this study, we have demonstrated the feasibility of selective mutant HTT lowering by miACTT2-451 construct delivered by the AAV5 vector in HD neuronal cultures heterozygous for  $\Delta$ ACTT. These results support further investigations using additional controls to provide the proof of mechanism and activity for the concept of miRNA-based transcript lowering in the nucleus.

## MATERIAL AND METHODS

### DNA plasmids

To generate the miACTT constructs, miACTT1 and miACTT2 guide sequences targeting HTT intron 22 pre-mRNAs were incorporated in the cellular pre-miRNA scaffolds of the human miR-101-1, miR-122, miR-135b, miR-155, and miR-451a scaffolds. 200 nucleotide-long 5' and 3' encompassing flanking regions were included with EcoRV and BamHI restriction sites and the full sequences were ordered from GeneArt® gene synthesis (Invitrogen, Carlsbad, CA). The constructs were expressed from the CAG promoter (Inovio, Plymouth Meeting, PA). The Mfold web server (<http://mfold.rna.albany.edu/?q=mfold>) was used to determine the pre-miACTT folding. For the generation of Luc-ACTT and Luc- $\Delta$ ACTT, a complete HTT intron 22 sequences containing either ACTT or  $\Delta$ ACTT, respectively, were cloned in the 3' UTR of the renilla luciferase gene of the psiCHECK-2 vector (Promega, Madison, WI, USA).

### AAV5 vector production

The AAV5-miACTT2 construct was produced by baculovirus-based AAV production system (uniQure, Amsterdam, The Netherlands) as previously described.<sup>10</sup> The miACTT2-451 expression cassette was inserted in a recombinant baculovirus vector by homologous recombination. The recombinant baculovirus was further amplified till the passage 6 and clones were screened for the best production and stability by PCR and qPCR. To generate AAV5, infections with different recombinant baculoviruses containing the vector genome, the replicon enzyme and the capsid protein were performed as described previously.<sup>10</sup>

### Transfections of HEK293T cells

HEK293T cells were maintained at 37°C and 5% CO<sub>2</sub> in Dulbecco's modified Eagle's medium (DMEM; Invitrogen) containing 10% fetal calf serum, 100 U/ml penicillin, and 100 U/ml streptomycin. For luciferase assays, cells were seeded in 24-well plates at  $1.2 \times 10^5$  per well and co-transfections were performed at 1:1 reporter:miACTT ratios. For qPCRs, HEK293T cells were seeded in 6-well plates at  $0.5 \times 10^5$  cells per well and co-transfections were performed at 2:1 reporter:miACTT ratios. For the next generation sequencing analysis, cells were seeded in 6-well plates at  $0.5 \times 10^5$  cells per well and 4  $\mu$ g of miACTT1-101 or miACTT2-451 was used for transfections. All transfections were performed with OptiMEM and Lipofectamine 2000 reagent according to manufacturer's instructions (Invitrogen).

### Luciferase assays

The luciferase assays were performed using Dual-Luciferase Reporter Assay System, according to the manufacturer's instructions (Promega, Madison, WI, USA). Two days post-transfection, HEK293T cells were lysed in 100  $\mu$ l 1x passive lysis buffer by gentle rocking for 15min at room temperature. The cell lysates were centrifuged for 5min at 4000rpm and

10 $\mu$ l of the supernatant was used to measure renilla and firefly activities. Relative luciferase activity was calculated as the ratio between renilla and firefly signals.

### **Separation of the nucleus and cytoplasm**

Two days post-transfection, the nucleus and cytoplasm were separated using Nuclei EZ Prep Isolation Kit according to the manufacturer's instructions (Sigma-Aldrich, St. Louis, Missouri, USA). Cells were washed with cold Dulbecco's PBS (Life Technologies, Carlsbad, CA, USA) and lysed using 500  $\mu$ l of Nuclei EZ lysis buffer. Nuclei were harvested by centrifugation at 500 x g for 5mins at 4°C. A supernatant containing the cytoplasmic fraction was collected in a separate tube and nuclei pellet was additionally washed with lysis buffer in order to remove cytoplasmic residues. Both nuclei and cytoplasmic fractions were ultimately resuspended in appropriate buffers and stored at -80°C.

### **Next generation sequencing**

Two days post-transfection, RNA was isolated from cells using Trizol according to the manufacturer's protocol (Invitrogen). Small RNA sequencing libraries for the Illumina sequencing platform were generated using the NEXTflex Small RNA Sequencing kit (Bio Scientific, Austin, TX, USA). The libraries were multiplexed, clustered, and sequenced on an Illumina HiSeq 2000 (TruSeq v3 chemistry) with a single-read 36 cycles sequencing protocol and indexing. The sequencing run was analyzed with the Illumina CASAVA pipeline (v1.8.2) with demultiplexing based on sample-specific barcodes. The raw sequencing data produced was processed removing the sequence reads which were of too low quality (only "passing filter" reads were selected). In total, we generated between 7-12 million reads per sample. The raw sequencing data were produced as previously described.<sup>11</sup> Small RNA raw data sets were analyzed using the CLC Genomics Workbench 6 (Qiagen, Hilden, Germany). The obtained unique small RNA reads were aligned to the reference sequences of the pre-miACTT1-101 and pre-miACTT2-451 constructs with a max. of three nucleotide mismatches allowed. The percentages of reads based on the total number of reads matching the reference sequences were calculated.

### **PCR and quantitative PCR**

Two days post-transfection, RNA was isolated from cells using Trizol according to the manufacturer's protocol (Invitrogen). To remove genomic DNA, RNA was treated with dsDNase (Thermo Scientific, Waltham, MA, USA). To measure mRNA knock-down and determine MAP2 expression, cDNA was generated using Maxima Synthesis Kit (Thermo Scientific). cDNA was analyzed by qPCR using custom probes named Ren/Intron\* and Intron\* and human GAPDH Hs02758991\_g1 (Thermo Scientific). Maturation status of neuronal cultures was evaluated by measuring expression of genes associated with neural development using TaqMan qPCR for detection of MAP2 Hs00258900\_m1 (Thermo

Scientific). To detect miACTT expression levels, RT-PCR and RT-qPCR were performed using TaqMan Fast Universal kit (Thermo Scientific). U6 snRNA (001973, Applied Biosystems) and custom miACTT probes for detection of mature miACTT1-101 and miACTT2-451 sequences were used (Thermo Scientific). The expression level of each gene was normalized to either endogenous GAPDH or U6 snRNA levels. Fold changes, percentages in mRNA knock-down, or miRNA expression were calculated based on  $2^{-\Delta\Delta CT}$  method.

### **Protein isolation and western blotting**

Protein content from nuclear and cytoplasmic fractions was isolated using RIPA lysis buffer (Sigma-Aldrich) supplemented with protein inhibitor cocktail (cOmplete™ ULTRA Tablet; Roche, Basel, Switzerland). Total protein concentration was quantified using a Bradford Protein Assay (Bio-Rad, Hercules, CA, USA) and absorbance was measured at 600 nm on the GloMax Discover System (Promega). Equal amounts of sample protein (10-30 µg) were incubated with β-mercaptoethanol and Laemmli buffer at 95°C for 5 min and separated using 4-20% Mini-Protean TGX Stain-Free Protein Gel (Bio-Rad). Samples were transferred to PVDF membranes by Trans-Blot Turbo Transfer system (Bio-Rad) using the "Mixed MW" protocol. Blot was incubated with 3% Blotting-Grade blocker (Bio-Rad) in 1x Tris Buffered Saline (TBS) for 1 hour at room temperature, followed by immunoblotting with selected primary antibody overnight at 4°C. Primary antibodies include the following: CD63 (System Biosciences), b-tubulin (Abcam), Actin (Abcam), Lamin B1 (Abcam) at 1:1000 dilution. Chromogenic signals were detected after 2 hours incubation with HRP-conjugated secondary antibodies (goat anti-rabbit, Abcam, 1:20000 or rabbit anti-mouse, Dako, Denmark, 1:20000) and 5 min incubation with SuperSignal Pico sensitivity Substrate (ThermoScientific) using ChemiDoc Touch Gel Imaging System (Bio-Rad).

### **Differentiation of forebrain HD neuronal cultures from human HD iPSCs**

HD iPSCs (CS97iHD-180n2) containing 180 CAG repeats were ordered from (Cedars-Sinai Medical Center, Los Angeles, CA, USA). These cells were generated from human HD fibroblasts GM09197 (Coriell Institute Stem Biobank, New Jersey, USA) reprogrammed with six factors (OCT4, SOX2, KLF4, LMYC, LIN28, shRNA to P53) using episomal vectors. As a negative control, HD iPSCs (ND42229\*B) containing 71 CAG repeats were ordered from (Coriell Institute Stem Biobank). These cells were generated from human HD fibroblasts GM04281 (Coriell Institute Stem Biobank) reprogrammed with six factors (OCT4, SOX2, KLF4, LMYC, LIN28, shRNA to P53) using episomal vectors. iPSCs were maintained on matrigel coating with mTeSR medium for several passages, following the manufacturer's instructions (StemCell Technologies, Vancouver, Canada). Non-differentiated colonies were released using ReLeSR reagent during each passage and diluted 1:5-20 (StemCell Technologies). For the neural induction, cells were plated onto AggreWell™ 800 plate at day 0 as 3x10<sup>6</sup> cells per well in STEMdiff™ Neural Induction Medium (StemCell Technologies). At day 5, embryoid

bodies were formed and replated onto poly-D-lysine/laminin coated 6-well plates. Coating was prepared with poly-D-lysine hydrobromide (0,1 mg/mL) and Laminin from Engelbreth-Holm-Swarm murine (0,1 mg/ml) (Sigma-Aldrich). At day 12, the neuronal rosettes were selected using STEMdiff™ Neural Rosette Selection Reagent (StemCell Technologies) and replated in poly-D-lysine/laminin coated plates. Next day, differentiation of neural progenitor cells was initiated using STEMdiff™ Neuron Differentiation Kit (StemCell Technologies). From day 19, cells were matured using STEMdiff™ Neuron Maturation Kit for a minimum of two weeks (StemCell Technologies).

### **SMC immunoassay for the mutant HTT protein quantification**

Protein lysates were resuspended in dilution buffer (50 µl/well) containing 6% BSA, 0.8% Triton X-100, 750 mM NaCl, and complete protease inhibitor (catalog 04693116001; Roche) and added to a 96-conical assay plate (catalog P-96-450V-C; Axygen). MAB2166 antibody (Merck Millipore) diluted to 1:1000 with Erenna Assay Buffer (02-0474-00; Singulex) coupled with magnetic particles (03-0077-02; Singulex) at a ratio of 25 µg antibody per milligram magnetic particles was added to the plate and shaking (600 rpm; Heidolph Titramax 1000 Microplate Shaker) at room temperature for 1 hour. The plate was placed on a magnetic rack and washed four times with 200 µl 1× washing buffer (02-0111-00; Singulex). 20 µl/well of 0.5 ng/µl diluted MW1 detection antibody labeled with detection fluorophore (catalog 03-0076-02; Singulex) at a ratio of 15.7 pmol fluorophore per micrgram MW1 was added to the plate. The plate was incubated shaking (750 rpm) at room temperature for 1 hour. Plates were washed, and the antibody-antigen complex was transferred to a new 96-conical assay plate. After four washes with 200 µl 1× washing buffer and aspiration, elution buffer (acidic glycine solution, 0.1 M, pH 2.7) was added to the plate, and the plate was incubated shaking (1,000 rpm) for 5 minutes. The eluted detection antibody was transferred to a Nunc 384-well analysis plate (catalog 264573; Sigma-Aldrich) and neutralized with neutralization buffer (Tris, 1 M, pH 9). The analysis plate was spun down, sealed, and subsequently analyzed with the Erenna Immunoassay System (Singulex).

### **Statistics**

Data were analyzed using un-paired Student's t-test (for two groups) or one-way ANOVA (for three or more groups) to determine statistical significances between samples. Tukey's post hoc test ( $\alpha=0.05$ ) was applied to analyzed differences between relevant groups. P-values are represented as: \* $p<0.05$ ; \*\* $p<0.01$ ; \*\*\* $p<0.001$ ; \*\*\*\* $p<0.0001$ .

## REFERENCES

1. Rawlins, MD, Wexler, NS, Wexler, AR, Tabrizi, SJ, Douglas, I, Evans, SJW, *et al.* (2016). The prevalence of huntington's disease. *Neuroepidemiology* **46**: 144–153.
2. Macdonald, ME, Ambrose, CM, Duyao, MP, Myers, RH, Lin, C, Srinidhi, L, *et al.* (1993). A Novel Gene Containing a Trinucleotide That Is Expanded and Unstable on Huntington's Disease Chromosomes. *Cell* **72**: 971–983.
3. Saudou, F and Humbert, S (2016). The Biology of Huntingtin. *Neuron* **89**: 910–926.
4. Bates, GP, Dorsey, R, Gusella, JF, Hayden, MR, Kay, C, Leavitt, BR, *et al.* (2015). Huntington disease. *Nat. Rev. Dis. Prim.* **1**: 1–21.
5. Marques Sousa, C and Humbert, S (2013). Huntingtin: Here, there, everywhere! *J. Huntingtons. Dis.* **2**: 395–403.
6. Ross, CA, Aylward, EH, Wild, EJ, Langbehn, DR, Long, JD, Warner, JH, *et al.* (2014). Huntington disease: natural history, biomarkers and prospects for therapeutics. *Nat. Rev. Neurol.* **10**: 204–16.
7. Mestre, TA and Sampaio, C (2017). Huntington Disease: Linking Pathogenesis to the Development of Experimental Therapeutics. *Curr. Neurol. Neurosci. Rep.* **17**: 1–8.
8. Difiglia, M, Sapp, E, Chase, KO, Davies, SW, Bates, GP, Vonsattel, JP, *et al.* (1997). Aggregation of huntingtin in neuronal intranuclear inclusions and dystrophic neurites in brain. *Science (80-. )*. **277**: 1990–3.
9. Davies, SW, Turmaine, M, Scherzinger, E, Wanker, EE, Mangiarini, L and Bates, GP (1997). Formation of Neuronal Intranuclear Inclusions Underlies the Neurological Dysfunction in Mice Transgenic for the HD Mutation. *Cell* **90**: 537–548.
10. Miniarikova, J, Zimmer, V, Martier, R, Brouwers, CC, Pythoud, C, Richetin, K, *et al.* (2017). AAV5-miHTT gene therapy demonstrates suppression of mutant huntingtin aggregation and neuronal dysfunction in a rat model of Huntington's disease. *Gene Ther.* **24**: 630–639.
11. Miniarikova, J, Zanella, I, Huseinovic, A, van der Zon, T, Hanemaaijer, E, Martier, R, *et al.* (2016). Design, Characterization, and Lead Selection of Therapeutic miRNAs Targeting Huntingtin for Development of Gene Therapy for Huntington's Disease. *Mol. Ther. Acids* **5**: e297.
12. Southwell, AL, Skotte, NH, Kordasiewicz, HB, Ostergaard, ME, Watt, AT, Carroll, JB, *et al.* (2014). In vivo evaluation of candidate allele-specific mutant huntingtin gene silencing antisense oligonucleotides. *Mol. Ther.* **22**: 2093–2106.
13. Harper, SQ, Staber, PD, He, X, Eliason, SL, Martins, IH, Mao, Q, *et al.* (2005). RNA interference improves motor and neuropathological abnormalities in a Huntington's disease mouse model. *Proc. Natl. Acad. Sci. U. S. A.* **102**: 5820–5825.
14. Sánchez, I, Mahlke, C and Yuan, J (2003). Pivotal role of oligomerization in expanded polyglutamine neurodegenerative disorders. *Nature* **421**: 373–379.
15. Ehrnhoefer, DE, Sutton, L and Hayden, MR (2011). Small changes, big impact: Posttranslational modifications and function of huntingtin in Huntington disease. *Neuroscientist* **17**: 475–492.
16. Kim, YJ, Yi, Y, Sapp, E, Wang, Y, Cuiffo, B, Kegel, KB, *et al.* (2001). Caspase 3-cleaved N-terminal fragments of wild-type and mutant huntingtin are present in normal and Huntington's disease brains, associate with membranes, and undergo calpain-dependent proteolysis. *Proc. Natl. Acad. Sci. U. S. A.* **98**: 12784–12789.
17. Wild, EJ and Tabrizi, SJ (2017). Therapies targeting DNA and RNA in Huntington's disease. *Lancet Neurol.* **16**: 837–847.
18. Evers, MM, Toonen, LJA and van Roon-Mom, WMC (2015). Antisense oligonucleotides in therapy for neurodegenerative disorders. *Adv. Drug Deliv. Rev.* **87**: 90–103.

19. Chery, J (2016). RNA therapeutics: RNAi and antisense mechanisms and clinical applications. *Postdoc J.* **4**: 35–50.
20. Miniarikova, J, Evers, MM and Konstantinova, P (2018). Translation of MicroRNA-Based Huntingtin-Lowering Therapies from Preclinical Studies to the Clinic. *Mol. Ther.* **26**: 947–962.
21. Kantor, B, McCown, T, Leone, P and Gray, SJ (2014). *Clinical applications involving CNS gene transfer. Adv. Genet.* **87**, Elsevier, 71-124pp.
22. Drouet, V, Perrin, V, Hassig, R, Dufour, N, Auregan, G, Alves, S, *et al.* (2009). Sustained effects of nonallele-specific Huntingtin silencing. *Ann. Neurol.* **65**: 276–85.
23. Cambon, K, Zimmer, V, Martineau, S, Gaillard, M, Jarrige, M, Bugi, A, *et al.* (2017). Preclinical Evaluation of a Lentiviral Vector for Huntingtin Silencing. *Mol. Ther. Methods Clin. Dev.* **5**: 259–276.
24. McBride, JL, Pitzer, MR, Boudreau, RL, Dufour, B, Hobbs, T, Ojeda, SR, *et al.* (2011). Preclinical Safety of RNAi-Mediated HTT Suppression in the Rhesus Macaque as a Potential Therapy for Huntington’s Disease. *Mol. Ther.* **19**: 2152–2162.
25. Stiles, DK, Zhang, Z, Ge, P, Nelson, B, Grondin, R, Ai, Y, *et al.* (2012). Widespread suppression of huntingtin with convection-enhanced delivery of siRNA. *Exp. Neurol.* **233**: 463–471.
26. Rasko, JEJ and Wong, JJ (2017). Nuclear microRNAs in normal hemopoiesis and cancer. *J. Hematol. Oncol.*: 1–8doi:10.1186/s13045-016-0375-x.
27. Jeffries, CD, Fried, HM and Perkins, DO (2011). Nuclear and cytoplasmic localization of neural stem cell microRNAs. *RNA* **17**: 675–686.
28. Roberts, TC (2014). The MicroRNA Biology of the Mammalian Nucleus. *Mol. Ther. - Nucleic Acids* **3**: e188.
29. Liao, JY, Ma, LM, Guo, YH, Zhang, YC, Zhou, H, Shao, P, *et al.* (2010). Deep sequencing of human nuclear and cytoplasmic small RNAs reveals an unexpectedly complex subcellular distribution of mirnas and tRNA 3’ trailers. *PLoS One* **5**: e10563.
30. Redfern, AD, Colley, SM, Beveridge, DJ, Ikeda, N, Epis, MR, Li, X, *et al.* (2013). RNA-induced silencing complex (RISC) Proteins PACT, TRBP, and Dicer are SRA binding nuclear receptor coregulators. *Proc. Natl. Acad. Sci. U. S. A.* **110**: 6536–41.
31. Wexler, NS, Young, AB, Tanzi, RE, Travers, H, Starosta-Rubinstein, S, Penney, JB, *et al.* (1987). Homozygotes for Huntington’s disease. *Nature* **326**: 194–7.
32. Kay, C, Skotte, N, Southwell, A and Hayden, M (2014). Personalized gene silencing therapeutics for Huntington disease. *Clin. Genet.* **86**: 29–36.
33. Cheloufi, S, Dos Santos, CO, Chong, MMW and Hannon, GJ (2010). A dicer-independent miRNA biogenesis pathway that requires Ago catalysis. *Nature* **465**: 584–589.
34. Cifuentes, D, Xue, H, Taylor, DW, Patnode, H, Mishima, Y, Cheloufi, S, *et al.* (2010). A novel miRNA processing pathway independent of Dicer requires Argonaute2 catalytic activity. *Science* **328**: 1694–1698.
35. Gagnon, KT, Li, L, Chu, Y, Janowski, BA and Corey, DR (2014). RNAi Factors are Present and Active in Human Cell Nuclei. *Cell Rep.* **6**: 211–221.
36. Jeffries, CD, Fried, HM and Perkins, DO (2011). Nuclear and cytoplasmic localization of neural stem cell microRNAs. *Spring*: 675–686doi:10.1261/rna.2006511.44.
37. Khudayberdiev, SA, Zampa, F, Rajman, M and Schrott, G (2013). A comprehensive characterization of the nuclear microRNA repertoire of post-mitotic neurons. *Front. Mol. Neurosci.* **6**: 1–19.
38. Gurtan, AM and Sharp, PA (2013). The role of miRNAs in regulating gene expression networks. *J. Mol. Biol.* **425**: 3582–3600.
39. Lochmatter, D and Mullis, P-E (2011). RNA interference in mammalian cell systems. *Horm. Res. paediatrics* **75**: 63–9.

40. Han, J, Lee, Y, Yeom, K-H, Kim, Y-K, Jin, H and Kim, VN (2004). The Drosha-DGCR8 complex in primary microRNA processing. *Genes Dev.* **18**: 3016–27.
41. Bohnsack, MT, Czaplinski, K and Görlich, D (2004). Exportin 5 is a RanGTP-dependent dsRNA-binding protein that mediates nuclear export of pre-miRNAs Exportin 5 is a RanGTP-dependent dsRNA-binding protein that mediates nuclear export of pre-miRNAs: 185-191doi:10.1261/rna.5167604.Most.
42. Chendrimada, TP, Gregory, RI, Kumaraswamy, E, Norman, J, Cooch, N, Nishikura, K, *et al.* (2005). TRBP recruits the Dicer complex to Ago2 for microRNA processing and gene silencing. *Nature* **436**: 740–4.
43. Gu, S, Jin, L, Zhang, Y, Huang, Y, Zhang, F, Valdmans, PN, *et al.* (2012). The loop position of shRNAs and pre-miRNAs is critical for the accuracy of Dicer processing in vivo. *Cell* **151**: 900–911.
44. Meijer, H a, Smith, EM and Bushell, M (2014). Regulation of miRNA strand selection: follow the leader? *Biochem. Soc. Trans.* **42**: 1135–40.
45. Yoda, M, Cifuentes, D, Izumi, N, Sakaguchi, Y, Suzuki, T, Giraldez, AJ, *et al.* (2013). Poly(A)-specific ribonuclease mediates 3'-end trimming of argonaute2-cleaved precursor micrornas. *Cell Rep.* **5**: 715–726.
46. Ma, H, Zhang, J and Wu, H (2014). Designing Ago2-specific siRNA/shRNA to Avoid Competition with Endogenous miRNAs. *Mol. Ther. Nucleic Acids* **3**: e176.
47. Harwig, A, Kruize, Z, Yang, Z, Restle, T and Berkhout, B (2017). Analysis of AgoshRNA maturation and loading into Ago2. *PLoS One*: 1–15.
48. Bartel, DP (2009). MicroRNAs: target recognition and regulatory functions. *Cell* **136**: 215–33.
49. Evers, MM, Miniarikova, J, Juhas, S, Vallès, A, Bohuslavova, B, Juhasova, J, *et al.* AAV5-miHTT gene therapy demonstrates broad distribution and strong human mutant huntingtin lowering in a Huntington disease minipig model: Submitted to Neuron.
50. Pfister, E, Dinardo, N, Mondo, E, Borel, F, Conroy, F, Fraser, C, *et al.* (2017). Artificial miRNAs reduce human mutant Huntingtin throughout the striatum in a transgenic sheep model of Huntington's disease. *Hum. Gene Ther.*doi:10.1089/hum.2017.199.
51. Tousley, A and Kegel-gleason, KB (2016). Induced Pluripotent Stem Cells in Huntington's Disease Research : Progress and Opportunity. *J. Huntingtons. Dis.* **5**: 99–131.